# Depth-resolved measurement of mucosal microvascular blood content using low-coherence enhanced backscattering spectroscopy

**Andrew J. Radosevich,[1,*] Vladimir M. Turzhitsky,[1] Nikhil N. Mutyal,[1] Jeremy D. Rogers,[1] Valentina Stoyneva,[1] Ashish Kumar Tiwari,[2] Mart De La Cruz,[2] Dhananjay P. Kunte,[2] Ramesh K. Wali,[2] Hemant K. Roy,[2] and Vadim Backman[1]**

[1]*Department of Biomedical Engineering, Northwestern University, Evanston, Illinois 60208, USA*
[2]*Department of Gastroenterology, Northshore University Healthsystems, Evanston, Illinois 60201, USA*
*\*andrewradosevich2014@u.northwestern.edu*

**Abstract:** Low-coherence enhanced backscattering (LEBS) spectroscopy is a light scattering technique which uses partial spatial coherence broadband illumination to interrogate the optical properties at sub-diffusion length scales. In this work, we present a post-processing technique which isolates the hemoglobin concentration at different depths within a sample using a single spectroscopic LEBS measurement with a fixed spatial coherence of illumination. We verify the method with scattering (spectralon reflectance standard and polystyrene microspheres) and absorbing (hemoglobin) phantoms. We then demonstrate the relevance of this method for quantifying hemoglobin content as a function of depth within biological tissue using the azoxymethane treated animal model of colorectal cancer.

## References and links

1. Y. L. Kim, Y. Liu, V. M. Turzhitsky, H. K. Roy, R. K. Wali, and V. Backman, "Coherent backscattering spectroscopy," Opt. Lett. **29**(16), 1906–1908 (2004).
2. V. Turzhitsky, J. D. Rogers, N. N. Mutyal, H. K. Roy, and V. Backman, "Characterization of Light Transport in Scattering Media at Subdiffusion Length Scales with Low-Coherence Enhanced Backscattering," IEEE J. Sel. Top. Quantum Electron. **16**(3), 619–626 (2010).
3. M. Albada, and A. Lagendijk, "Observation of weak localization of light in a random medium," Phys. Rev. Lett. **55**(24), 2692–2695 (1985).
4. E. Akkermans, P. E. Wolf, and R. Maynard, "Coherent backscattering of light by disordered media: Analysis of the peak line shape," Phys. Rev. Lett. **56**(14), 1471–1474 (1986).
5. M. I. Mishchenko, "Enhanced Backscattering of Polarized-Light from Discrete Random-Media - Calculations in Exactly the Backscattering Direction," J. Opt. Soc. Am. A **9**(6), 978–982 (1992).
6. M. Born, E. Wolf, and A. B. Bhatia, *Principles of Optics: Electromagnetic Theory of Propagation, Interference and Diffraction of Light,* 7th (expanded) ed. (Cambridge University Press, New York, 1999), pp. xxxiii.
7. M. Xu, "Low-coherence enhanced backscattering beyond diffusion," Opt. Lett. **33**(11), 1246–1248 (2008).
8. C. Schwartz, and A. Dogariu, "Enhanced backscattering of vortex waves from volume scattering media," Opt. Commun. **263**(2), 135–140 (2006).
9. W. F. Cheong, S. A. Prahl, and A. J. Welch, "A Review of the Optical-Properties of Biological Tissues," IEEE J. Quantum Electron. **26**(12), 2166–2185 (1990).
10. G. I. Zonios, R. M. Cothren, J. T. Arendt, J. Wu, J. VanDam, J. M. Crawford, R. Manoharan, and M. S. Feld, "Morphological model of human colon tissue fluorescence," IEEE Trans. Bio-Med. Eng. **43**, 113–122 (1996).
11. J. C. Ramella-Roman, S. A. Prahl, and S. L. Jacques, "Three Monte Carlo programs of polarized light transport into scattering media: part I," Opt. Express **13**(12), 4420–4438 (2005).
12. J. C. Ramella-Roman, S. A. Prahl, and S. L. Jacques, "Three Monte Carlo programs of polarized light transport into scattering media: part II," Opt. Express **13**(25), 10392–10405 (2005).

13. H. Subramanian, P. Pradhan, Y. Kim, and V. Backman, "Penetration depth of low-coherence enhanced backscattering of light in sub-diffusion regime," Phys. Rev. E Stat. Nonlin. Soft Matter Phys. **75**(041914), 1–9 (2007).
14. V. M. Turzhitsky, A. J. Gomes, Y. L. Kim, Y. Liu, A. Kromine, J. D. Rogers, M. Jameel, H. K. Roy, and V. Backman, "Measuring mucosal blood supply in vivo with a polarization-gating probe," Appl. Opt. **47**(32), 6046–6057 (2008).
15. S. A. Prahl, M. J. C. van Gemert, and A. J. Welch, "Determining the optical properties of turbid mediaby using the adding-doubling method," Appl. Opt. **32**(4), 559–568 (1993).
16. S. Prahl, "Tabulated molar extinction coefficient for hemoglobin in water," *http://omlc.ogi.edu/spectra/hemoglobin/summary.html* (1998).
17. M. Hunter, V. Backman, G. Popescu, M. Kalashnikov, C. W. Boone, A. Wax, V. Gopal, K. Badizadegan, G. D. Stoner, and M. S. Feld, "Tissue self-affinity and polarized light scattering in the born approximation: a new model for precancer detection," Phys. Rev. Lett. **97**(13), 138102 (2006).
18. J. D. Rogers, I. R. Capoğlu, and V. Backman, "Nonscalar elastic light scattering from continuous random media in the Born approximation," Opt. Lett. **34**(12), 1891–1893 (2009).
19. A. J. Gomes, H. K. Roy, V. Turzhitsky, Y. Kim, J. D. Rogers, S. Ruderman, V. Stoyneva, M. J. Goldberg, L. K. Bianchi, E. Yen, A. Kromine, M. Jameel, and V. Backman, "Rectal mucosal microvascular blood supply increase is associated with colonic neoplasia," Clin. Cancer Res. **15**(9), 3110–3117 (2009).
20. H. K. Roy, A. Gomes, V. Turzhitsky, M. J. Goldberg, J. Rogers, S. Ruderman, K. L. Young, A. Kromine, R. E. Brand, M. Jameel, P. Vakil, N. Hasabou, and V. Backman, "Spectroscopic microvascular blood detection from the endoscopically normal colonic mucosa: biomarker for neoplasia risk," Gastroenterology **135**(4), 1069–1078 (2008).
21. H. K. Roy, A. J. Gomes, S. Ruderman, L. K. Bianchi, M. J. Goldberg, V. Stoyneva, J. D. Rogers, V. Turzhitsky, Y. Kim, E. Yen, M. Jameel, A. Bogojevic, and V. Backman, "Optical measurement of rectal microvasculature as an adjunct to flexible sigmoidosocopy: gender-specific implications," Cancer Prev Res (Phila) **3**(7), 844–851 (2010).
22. R. K. Wali, H. K. Roy, Y. L. Kim, Y. Liu, J. L. Koetsier, D. P. Kunte, M. J. Goldberg, V. Turzhitsky, and V. Backman, "Increased microvascular blood content is an early event in colon carcinogenesis," Gut **54**(5), 654–660 (2005).
23. A. Banerjee, and P. Quirke, "Experimental models of colorectal cancer," Dis. Colon Rectum **41**(4), 490–505 (1998).
24. J. C. Finlay, and T. H. Foster, "Effect of pigment packaging on diffuse reflectance spectroscopy of samples containing red blood cells," Opt. Lett. **29**(9), 965–967 (2004).
25. G. Zonios, L. T. Perelman, V. M. Backman, R. Manoharan, M. Fitzmaurice, J. Van Dam, and M. S. Feld, "Diffuse reflectance spectroscopy of human adenomatous colon polyps in vivo," Appl. Opt. **38**(31), 6628–6637 (1999).
26. M. Brittan, and N. A. Wright, "Stem cell in gastrointestinal structure and neoplastic development," Gut **53**(6), 899–910 (2004).
27. S. L. Preston, W. M. Wong, A. O. O. Chan, R. Poulsom, R. Jeffery, R. A. Goodlad, N. Mandir, G. Elia, M. Novelli, W. F. Bodmer, I. P. Tomlinson, and N. A. Wright, "Bottom-up histogenesis of colorectal adenomas: origin in the monocryptal adenoma and initial expansion by crypt fission," Cancer Res. **63**(13), 3819–3825 (2003).
28. L. H. Wang, S. L. Jacques, and L. Q. Zheng, "MCML--Monte Carlo modeling of light transport in multi-layered tissues," Comput. Methods Programs Biomed. **47**(2), 131–146 (1995).

## 1. Introduction

The ability to acquire depth-resolved measurements of the optical scattering and absorption properties within biological tissue at sub-diffusion length scales can provide an invaluable tool for studying the structure and composition of the superficial layers of tissues. One way to achieve this selectivity is through use of coherence gating methods such as low-coherence enhanced backscattering (LEBS) [1]. The LEBS signal is generated by the interference pattern formed by photons traveling time-reversed paths, and manifests itself as an intensity peak centered in the exact backscattering direction. Through use of illumination with partial spatial coherence, the contribution from path pairs which exit the medium at radial separations exceeding the spatial coherence length is greatly reduced. Since photons which exit the medium at large radial distances from their entrance point tend to travel deeper within the medium, this in turn restricts the depth from which the LEBS signal is collected. By varying the degree of spatial coherence, it is therefore possible to interrogate the optical properties from within different depths of a sample.

In addition to its depth selectively, another advantage of LEBS is its use of broadband illumination which allows spectroscopic analysis of the signal. If the shape of the absorption

spectrum for all chromophores within a sample is known *a priori,* the scattering and absorption components of the LEBS spectrum can be separated. This provides a method for quantifying the concentrations of absorbers (such as hemoglobin) within the scattering medium.

Previously, LEBS depth selectivity has only been achieved by physically changing the spatial coherence length ($L_{sc}$) of illumination, a process that is time consuming and requires system recalibration. However, in this work we demonstrate that all the information needed to accurately reconstruct the LEBS peak shape for a wide range of tissue depths can be obtained from the measurement at a single $L_{sc}$ (which restricts the maximum penetration depth from which the signal can be obtained). We first present a post-processing method for reconstructing the LEBS peak shape for shallower depths and provide verification of its accuracy using purely scattering phantoms. We then demonstrate this method for spectral measurements, and use an algorithm based on the Beer-Lambert law to quantify hemoglobin concentration using the LEBS spectrum. Finally, we demonstrate this technique for biological tissue characterization using a carcinogen treated animal model of colon cancer.

## 2. Materials and methods

### 2.1 Theoretical background

The shape of the LEBS intensity peak is determined by two independent components: the impulse response radial reflectance profile of light in the exact backward direction, *p(r),* and the normalized mutual intensity (alternatively known as the degree of spatial coherence) of the illumination, *c(r)* [2]. It is important to note that *p(r)* is a completely sample dependent parameter, and does not change when observed with different *c(r).* Under perfectly spatially coherent illumination (i.e. when *c(r)* = 1 at all radial separations), the intensity peak has been well studied under the names of coherent backscattering (CBS) and enhanced backscattering (EBS) [3–5]. In this case, the intensity peak can be thought of as the summation of the diffraction patterns from many different double pinhole arrangements, where the weighting of various pinhole separations is specified by *p(r).* The resulting intensity peak can therefore be found by computing the two dimensional Fourier transform of *p(r).* Under partial spatial coherence illumination, *c(r)* acts as a spatial filter that limits the contribution of the time-reversed photon pairs exiting at larger radial separations from each other. Accordingly, the observed peak will be the two dimensional Fourier transform of *p(r)* multiplied by the *c(r)* filter:

$$I_{LEBS}(\theta) = FT\big[p(r) \cdot c(r)\big] \qquad (1)$$

Photon pairs that exit a medium at larger radial separations tend on average to penetrate deeper into a sample. Therefore, *c(r)* restricts the penetration depth of the signal by limiting the radial contribution of LEBS photons. Since *p(r)* is sensitive to both the scattering and absorption properties of a sample, this provides an excellent tool for optically interrogating the most superficial depths of tissue.

### 2.2 LEBS instrumentation

The LEBS instrument is shown in Fig. 1(a). A 450W Xenon lamp (Oriel Instruments) is focused onto an aperture wheel with six high power tungsten apertures (Lenox Laser) with diameters ranging from 0.25 – 1.75 mm. The incoherent light emitted by the aperture gains spatial coherence as it propagates through the air until it is collimated by a lens ($f$ = 200mm). Assuming a perfectly circular source intensity distribution, the normalized mutual intensity of the collimated light is given by [2,6]:

$$c(r) = \frac{2J_1(r/L_{sc})}{r/L_{sc}} \qquad (2)$$

$$L_{sc} = \frac{f}{ka} \qquad (3)$$

where $J_1$ is the first-order Bessel function of the first kind, $k$ is the wave number, $a$ is the radius of the aperture, and $f$ is the focal length of the collimating lens. The spatial coherence length, $L_{sc}$, is defined as the point at which $c(r)$ reaches a value of 0.88. The partially coherent illumination then passes through a linear polarizer and is directed by a beamsplitter onto the sample. An iris before the beamsplitter limits the beam spot size to 4 mm in diameter. The backscattered light travels through a co-polarized linear analyzer and is focused onto a CCD camera (PIXIS 400B, Princeton Instruments) by an achromatic lens ($f = 100$mm). A liquid crystal tunable filter (CRi instruments) with a bandwidth of 20 nm (full width at half maximum) is used to separate the backscattered light into its component wavelengths. This design can map the LEBS intensity peak for angles up to 2.18 degrees from the exact backscattering direction with a resolution of 0.0115 degrees.

In order to process the data, measurements are first background subtracted and divided by a flat field to remove artifacts caused by the camera imaging system. The LEBS peak is then obtained by subtracting the incoherent baseline intensity and dividing by the total diffuse intensity as measured by a spectralon reflectance standard (Ocean Optics). Characterization of the shape of the peak is then determined by the enhancement factor $E$ (the height of the peak as a ratio to the total diffuse intensity) and width (full width at half maximum). The enhancement factor is related to the reduced scattering coefficient, $\mu_s^*$, by [2,7]:

$$E = c \cdot \mu_s^* L_{sc} \qquad (4)$$

Although the prefactor, $c$, depends on the optical properties, it can be approximated as 0.2 within the range of optical properties expected in tissue [2].

Verification of the $c(r)$ from each aperture was carried out by measuring the angular intensity distribution from each tungsten aperture secondary source. According to the van Cittert-Zernike theorem, $c(r)$ is the normalized Fourier transform of the angular intensity distribution of the source (assuming that $a \ll f$ and the illumination at the source is completely incoherent) [6]. The source distribution is easily measured by placing a mirror in the sample plane and imaging the aperture onto the CCD. As an additional measure, $c(r)$ was confirmed by measuring the interference pattern from four different double slit configurations with slit separations of 50, 100, 200, and 400 μm. Figure 1(b) shows the agreement between the theoretical $c(r)$ given by Eq. (2) and the experimentally measured $c(r)$ at 700 nm. Fitting the shape of the experimental $c(r)$ to the theoretical $c(r)$ gives an error of 2.60% ± 1.69% (average ± standard deviation) between the six apertures.
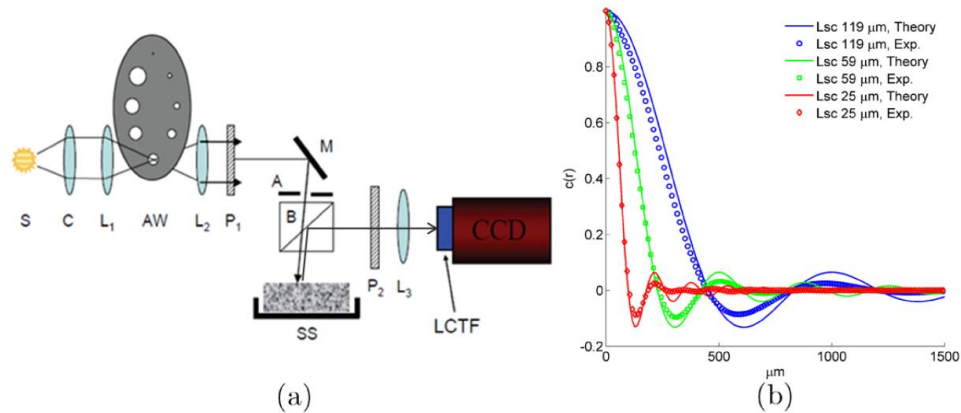
Fig. 1. **[a]** Schematic of the LEBS instrumentation. S: Broadband Xenon illumination source, C: condenser, L1-L3: lenses, AW: aperture wheel, P1-P2: polarizers, M: mirror, A: iris aperture, B: beamsplitter, SS: sample, LCTF: liquid crystal tunable filter. Aperture AW contains 6 different tungsten apertures which determine the spatial coherence of illumination, P1 and P2 act as a polarizer and analyzer, respectively. **[b]** Comparison of the shape of the experimentally measured $c(r)$ versus those predicted by the van Cittert-Zernike theorem for 3 different example $L_{sc}$.

## 2.3 Post-processing reconstruction technique

As has been discussed above, LEBS measurements at different $L_{sc}$ can be acquired by physically changing the radius of the tungsten aperture in the aperture wheel [Fig. 1(a)]. Throughout the rest of this text, we refer to LEBS peaks measured in this way as being 'experimentally measured'. In this section we present a post-processing method which can be used to accurately reconstruct the shape of a wide range of experimentally measured LEBS peaks from the experimental measurement of an LEBS peak at a single $L_{sc}$. We refer to LEBS peaks generated in this way as being 'reconstructed'. To accomplish the reconstruction we must first recover $p(r)$ from an experimentally measured LEBS peak.

Expressing Eq. (1) in an alternative way, $p(r)$ can be determined if we measure an experimental LEBS peak and the shape of $c(r)$ is well known:

$$p(r) = \frac{FT^{-1}[I_{LEBS}(\theta)]}{c(r)} \tag{5}$$

This measurement of $p(r)$ comes with the caveat that radial separations around the zeros of $c(r)$ cannot be measured since the value of $p(r)$ after dividing by zero will falsely appear to approach infinity. In order to remove these aberrant data points, the values of $p(r)$ at $\pm 15$ µm around the zeros of $c(r)$ are set to a value of 0. Figure 2 shows an example of an experimentally measured $p(r)$ before removal of the aberrant peaks caused by the zeros of $c(r)$. While this means that we cannot acquire a perfect $p(r)$ at all radial separations, this effect does not contribute much error to the reconstructed peak shape since with decreasing $L_{sc}$, the bulk of the weight of $c(r)$ will be located at small radial separations, thus largely avoiding contribution from the zeroed values. In addition to removing points around the zeros of $c(r)$, the experimental LEBS image is zero-padded (i.e. increasing the angular extent of the data array by appending zeros to its periphery) prior to computing the inverse Fourier transform. Zero-padding in the frequency domain results in an ideal interpolation in the spatial domain. Since $p(r)$ is a smoothly varying function, zero-padding the LEBS peak increases the resolution of $p(r)$ without altering its shape and helps improve algorithm accuracy.

After recovering $p(r)$, the LEBS peak at different $c(r)$ can be reconstructed according to Eq. (1) by assuming new theoretical $c(r)$ functions with different $L_{sc}$ values. Since photons

exiting at radial distances outside of the coherence area cannot contribute significantly to the LEBS peak, the reconstruction can only be carried out accurately for $L_{sc}$ shorter than the experimentally measured $L_{sc}$. The light blue lines in Fig. 1 provide an example of the $c(r)$ with smaller $L_{sc}$ for which we can reconstruct the LEBS peak.
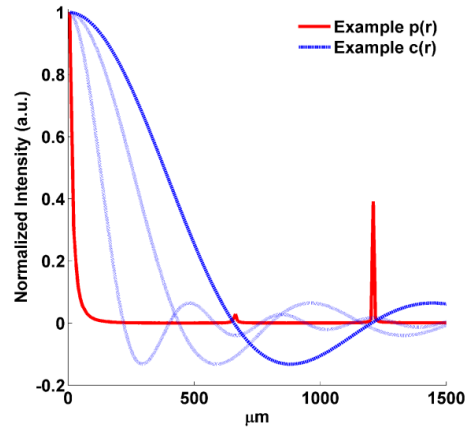


Fig. 2. Example of the radially averaged and maximum-normalized experimentally measured $p(r)$ [red] as well as the $c(r)$ [blue] used for its recovery from the LEBS peak. The light blue lines represent the $c(r)$ with smaller $L_{sc}$ that can be used to reconstruct the LEBS peak.

## 3. Experimental validation

### 3.1 Scattering tissue models

As an initial verification of the reconstruction algorithm, we acquired experimental LEBS readings at 680 nm from the highly scattering (transport mean free path, ls* ~20 μm) [8] spectralon reflectance standard used for calibration. In order to verify the accuracy of the reconstructed LEBS peak values, we took 10 measurements from each of the six different experimental $L_{sc}$ of illumination. We then used the measurement from the longest $L_{sc}$ (173 μm) to reconstruct the LEBS peak at the six experimental $L_{sc}$. The results, which are summarized in Fig. 3, demonstrate an excellent agreement between the shape of the reconstructed peak and the experimental measurements acquired by physically changing the $L_{sc}$ through a repositioning of the aperture wheel. The enhancement factor [Fig. 3(a)] was reconstructed with an average error versus the six experimental $L_{sc}$ of 1.07% ± 1.05% while the width [Fig. 3(b)] had error of 1.31% ± 1.03%. In addition, the standard deviation [Fig. 3(c)] between the 10 measurements tended to decrease with decreasing $L_{sc}$. This shows that the reconstruction does not add any variability to the measured values, and in fact even decreases the variability as the reconstructed $L_{sc}$ becomes much less than the initially measured $L_{sc}$.

In addition to the spectralon reflectance standard, a purely scattering (no absorption) sample composed of monodispersed polystyrene microspheres was used to validate the reconstruction algorithm for the ls* and anisotropy factor (g) in the regime expected for mucosal tissue [9,10]. In order to recreate the scattering properties of tissue, a suspension of microspheres with 0.65 μm diameter was used. Calculation of the optical properties was carried out according to Mie theory and yielded a g of 0.86 and ls* of 804 μm at 680 nm illumination. The sample thickness was maintained at greater than 10 times ls* to approximate a semi-infinite medium. Comparison between the reconstructed and experimental LEBS peak parameters were conducted as with the reflectance standard. As a method to verify both results versus theory, a polarized light Monte Carlo simulation of $p(r)$ using the Mie phase function for the corresponding sphere size was used [2,11–13]. The theoretical LEBS peak was then calculated from the simulated $p(r)$ according to Eq. (1).

The results, which are summarized in Fig. 4 show excellent agreement between the reconstructed and experimentally measured parameters. An average error of 3.74% ± 2.46% and 2.60% ± 1.90% versus the experimentally measured $L_{sc}$ was seen for the enhancement and width, respectively. Matching with the theoretically predicted peaks from Monte Carlo, we measured an average error of 1.48% ± 1.55% and 4.61% ± 2.10% for the enhancement and width, respectively. The standard deviation of the width across the 10 realizations increased slightly for shorter $L_{sc}$, but stayed within the same order of magnitude, while the standard deviation of the enhancement decreased for shorter $L_{sc}$.
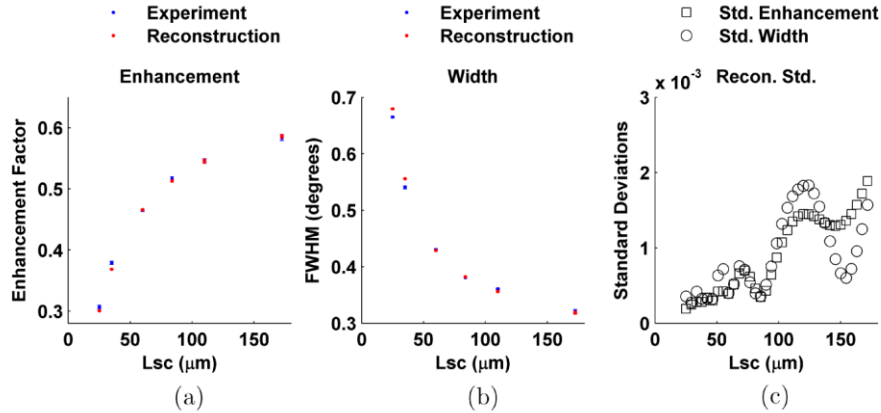


Fig. 3. Demonstration of the accuracy of the reconstruction technique for recovering the LEBS peak shape at different $L_{sc}$ using the spectralon reflectance standard. **[a,b]** shows the comparison between the reconstructed and experimentally measured LEBS peaks. **[c]** shows the standard deviation between 10 measurements at different reconstructed $L_{sc}$.
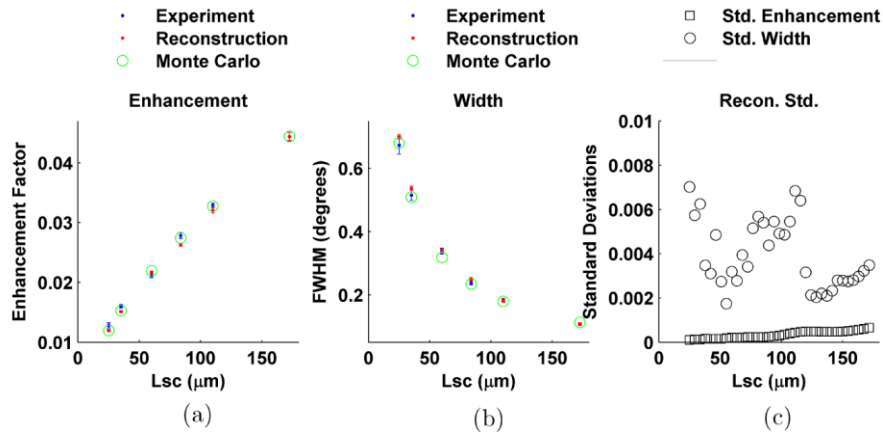


Fig. 4. Demonstration of the accuracy of the reconstruction technique for recovering the LEBS peak shape at different $L_{sc}$ using a tissue simulating phantom composed of polystyrene microspheres. **[a,b]** shows the comparison between the reconstructed and experimentally measured LEBS peaks. **[c]** shows the standard deviation between 10 measurements at different reconstructed $L_{sc}$.

*3.2 Absorption quantification*

Validation of the reconstruction technique for quantifying optical absorption was carried out by constructing scattering and absorbing phantoms from a 20% fat emulsion Intralipid (I141 Sigma-Aldrich) with varying concentrations of hemoglobin (HO267 Sigma-Aldrich) in the physiological range (3 - 15 g/L) [14]. The Intralipid was diluted in PBS to obtain a tissue-

relevant ls* of ~700 μm which was confirmed with integrating sphere measurements [15]. Spectral LEBS measurements were acquired by tuning the spectrometer wavelength between 500 and 600 nm with a 4 nm step size. Plotting the LEBS enhancement factor vs. wavelength reveals the sample's spectrum with distinctive hemoglobin absorption bands around 542 and 576 [Fig. 5(a)]. In order to separate the scattering and absorption components of the spectrum, we implemented an algorithm based on the Beer-Lambert law [14]:

$$E(\lambda) = E_{scattering}(\lambda) \cdot \exp(-\mu_{eff}(\lambda)) \tag{6}$$

$$\mu_{eff}(\lambda) = \sum_i \alpha_i \cdot A_i(\lambda) \tag{7}$$

where $E_{scattering}(\lambda)$ is the purely scattering spectrum of the sample that would be recorded if the medium were devoid of absorption, $\mu_{eff}$ is the effective attenuation due to all absorbing species within the sample, $\alpha_i$ is the product of absorber concentration and path length, and $A_i(\lambda)$ is the absorption spectrum. When there are multiple absorbers within a sample, $\mu_{eff}$ is the linear sum of $\alpha_i$ multiplied by $A_i(\lambda)$ for each absorbing component within the sample. In the case of hemoglobin, the absorption spectra for both the oxygenated (OHb) and de-oxygenated (DHb) molecule must be considered. Values of the hemoglobin absorption spectra were compiled from a published online source [16]. In order to account for the 20 nm bandwidth of the spectrometer, the published spectra were convolved with a Gaussian function with a FWHM of 20 nm.

Although the purely scattering portion of the LEBS enhancement spectrum is not known *a priori*, it can be inferred by assuming that $\mu_s*$ is proportional to $\lambda^{2m-4}$. This relation is derived by applying the Born approximation to the Whittle-Mattérn family of correlation functions, in which *m* is a parameter that determines the shape of the refractive index correlation function for a continuous random medium [17,18]. When $m < 1.5$, the function corresponds to a mass fractal distribution in which the fractal dimension is *2m*. Relating the enhancement factor to $\mu_s*$ through Eq. (4) and adjusting for the wavelength dependence of $L_{sc}$, the enhancement scattering spectrum will then follow the form:

$$E_{scattering}(\lambda) \propto \lambda^{2m-3} \tag{8}$$

In order to determine the values of *m* and $\alpha_i$ that provide the best fit to the experimental data, we iteratively minimize the sum of the squared error between the assumed scattering spectrum with absorption added and the experimentally observed spectrum using the built-in Matlab (MathWorks Inc) function fminsearch.

By carrying out the reconstruction technique over a range of wavelengths from 500 to 600 nm, we are able to accurately recreate and quantify the absorption spectra observed from the experimental measurements. Figure 5(a) shows the reconstructed spectra and the corresponding fit predicted by the model used to extract the α values. As $L_{sc}$ increases, the average path length of the photons that contribute to the enhancement also increases. This results in the observed deepening of the absorption dips in the spectra with increasing $L_{sc}$ as indicated by the black arrows in Fig. 5(a). Figure 5(b) shows the best fit α values across the reconstructed $L_{sc}$ for both OHb and DHb where the $L_{sc}$ is defined at the central wavelength of 550 nm. The α values for OHb were reconstructed with an average error of 4.23% ± 2.87% versus the experimental measurement. While the experimental measurement of $\alpha_{OHb}$ for $L_{sc}$ smaller than 20 μm is not possible with our current system, the shape of the reconstruction curve follows the expected trend. At larger $L_{sc}$, the measurement approaches a plateau level as the path length of photons contributing to the enhancement reaches a saturation point corresponding to the EBS regime (i.e. $L_{sc} > $ ls*). The measured $\alpha_{DHb}$ value was negligibly small, since in an open air environment hemoglobin assumes its oxidized form. While this result is expected, it confirms that the absorption quantification algorithm is robust.
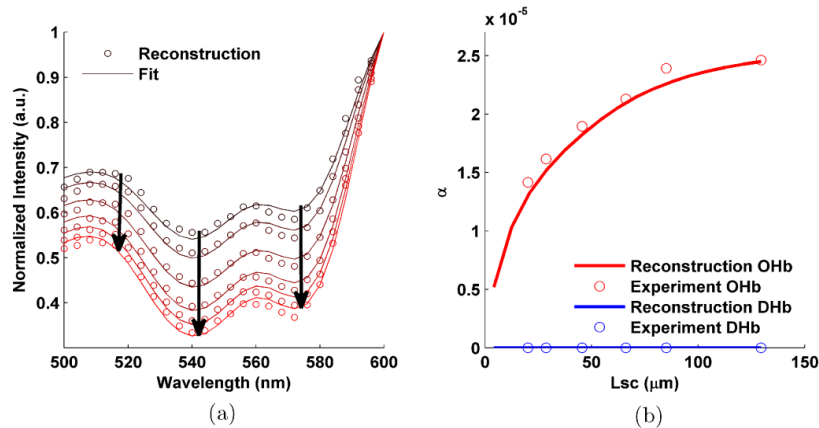
Fig. 5. **[a]** shows the reconstructed absorption spectra normalized by the value at 600 nm. The arrows indicate increasing $L_{sc}$. **[b]** shows the comparison between the experimentally measured and reconstructed values of α for both OHb and DHb.

In order to quantify the concentration of hemoglobin, a calibration curve for each $L_{sc}$ was generated using the reconstructed α values from samples of varying hemoglobin concentration [as shown in Fig. 6(a)]. Using this method, the hemoglobin concentration can be accurately determined for a wide range of $L_{sc}$ with greatly differing average photon path lengths. For each of the four $L_{sc}$ shown in Fig. 6(b), the average error of hemoglobin measurements was determined to be less than 5% within the tissue-relevant range of concentrations.
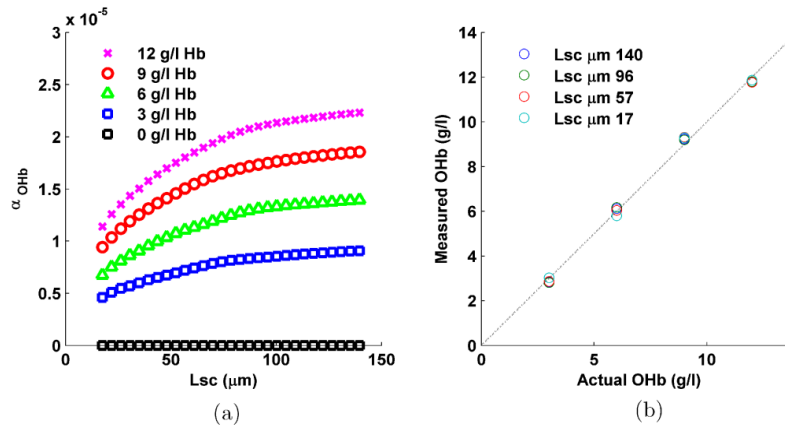


Fig. 6. **[a]** shows the reconstructed $\alpha_{OHb}$ values across $L_{sc}$ for different concentrations of hemoglobin in the physiological range. **[b]** shows the comparison between the $\alpha_{OHb}$ values measured from the calibration curves constructed for 4 different examples of $L_{sc}$.

### 3.3 Two-layer phantom

In order to verify the relevance of our method for quantifying hemoglobin in layered media we performed a series of experiments on two-layer phantoms. To construct a two-layer phantom we used a liquid Intralipid bottom layer with ls* ~700 µm and 10 g/L hemoglobin concentration. We then placed a solid silicone (Sylgard® 182 silicone elastomer, Dow Corning) film containing titanium dioxide scatterers (T8141, Sigma-Aldrich) with ls* = 135 µm over the liquid Intralipid-hemoglobin mixture and took spectral measurements as described above. Figure 7(a) shows the $\alpha_{OHb}$ curves across $L_{sc}$ (normalized to the value at 74 µm $L_{sc}$) for film layers of 25, 50, and 75 µm thickness. The effect of the thin scattering slice is

to create a horizontal offset in the $\alpha_{OHb}$ curve. This occurs because at shorter $L_{sc}$, the photons contributing to the LEBS enhancement spectrum travel only through the scattering layer and do not exhibit the absorption property of the second layer. As $L_{sc}$ increases, the absorption in the second layer begins to contribute to the spectrum; however the path length of photons traveling through the second layer is reduced by the top layer, thus leading to an offset in the curve. Each additional layer contributes an offset of ~15 $L_{sc}$, with the 25, 50, and 75 μm slices' $\alpha_{OHb}$ values reaching 0 at $L_{sc}$ of 15, 29, and 44 μm, respectively.

Figure 7(b) shows the purely scattering spectrum isolated from a 100 μm slice at a reconstructed $L_{sc}$ of 44 μm. After reconstructing the same experimental measurement at an $L_{sc}$ of 128 μm, the two characteristic OHb absorption dips can be seen in the spectrum. This confirms that we are able to extract the spectrum corresponding to two different layers within a sample by reconstructing the LEBS peak from a single spectral experimental measurement.
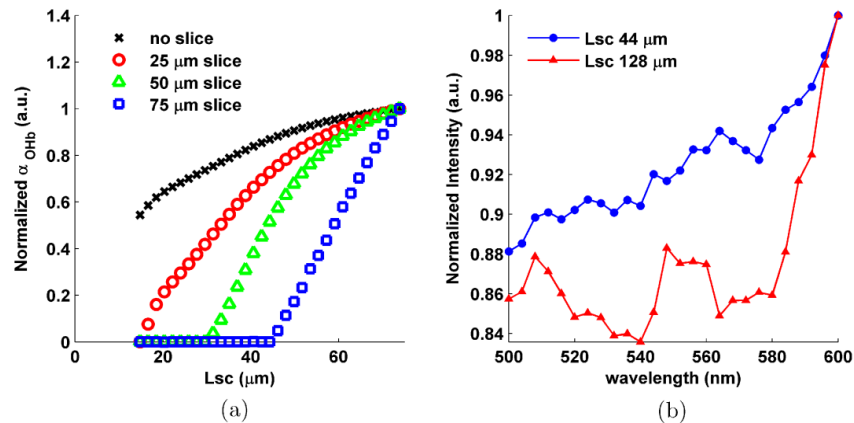


(a)                                        (b)

Fig. 7. **[a]** shows the normalized $\alpha_{OHb}$ values across different $L_{sc}$ for two layer phantoms with a superficial scattering layer of 25, 50, and 75 μm. **[b]** shows an example of the spectrum isolated from the purely scattering top layer by reconstructing the spectrum at 44 μm $L_{sc}$ [blue] as well as the spectrum from a larger $L_{sc}$ of 128 μm [red] which penetrates into the second scattering and absorbing layer. Both spectra were reconstructed from a single experimental measurement.

## 4. Application: depth-selective measurement of mucosal blood supply in an animal model of colon carcinogenesis

During the development of cancer, an increase in mucosal blood supply is seen as the diseased tissue becomes increasingly metabolically active. As such the detection of this increase in blood supply provides a useful biomarker of cancer, which can be used for optical cancer screening [14,19–22]. However, the location and origin of these changes is still not well understood. As a demonstration of the relevance of the post-processing algorithm that we have outlined in this work, we reconstruct the location and concentration of this increase in mucosal microvasculature.

Blood supply in early colon carcinogenesis was studied using the azoxymethane (AOM)-treated rat model of colon carcinogenesis with a saline-treated control group. 18 Fisher 344 rats (150–200 g; Harlan, Indianapolis, IN) were treated with two weekly Intraperitoneal (i.p.) injections of either 15 mg/kg AOM or saline. Animals were euthanized 10 weeks after the second AOM injection. This is an early time point that follows the development of aberrant crypt foci (~5-8 weeks) but precedes the appearance of adenomas (~20 weeks) and carcinomas (~40 weeks) [23]. The colons were removed, opened longitudinally, and washed prior to taking LEBS measurements. All animal procedures were reviewed and approved by the Institutional Animal Care and Use Committee for NorthShore University HealthSystem.

Spectral LEBS measurements were acquired between 500 and 700 nm with a 20 nm step. At the largest $L_{sc}$ of 153 μm (at 600 nm) a spectral measurement with sufficiently low noise level was acquired from a single tissue location in 11 minutes. 10 evenly spaced measurements over a 1 inch segment of the distal colon were measured for each animal. Prior to fitting the hemoglobin spectrum using the previously described method, the absorption spectra were first corrected for hemoglobin packing in blood vessels according to the method described by Finlay and Foster [14,24]. The average penetration depth of all photons contributing to the LEBS spectrum was determined by reconstructing the peak between 600 and 700 (a range where hemoglobin absorption is low) and calculating $\mu_s*$ for each $L_{sc}$ according to Eq. (4) and assuming a $g$ of 0.9 [13]. Hemoglobin concentrations were determined by dividing the $\alpha_{THb}$ value by the total path length. Neglecting the lateral translation of the light, the path length was approximated as twice the penetration depth [14].

The results of the animal study are summarized in Fig. 8. The total hemoglobin (THb) concentration values found by summing the contribution from OHb and DHb represent the total blood content of the colon tissue. For these specimens, the absorption due to OHb was negligibly small while the main effect was seen with DHb as a result of euthanasia. The α value curve shown in Fig. 8(a) exhibits the same plateauing shape seen from liquid Intralipid-hemoglobin phantom. However, due to the multilayered structure of the tissue, this shape can be attributed to both a change in path length and hemoglobin concentration. Removing the path length contribution, Fig. 8(b) shows the depth-resolved measurement of THb concentrations. The absolute values are similar to those found by Zonios *et al* in human colon mucosa [25]. The relative change in concentration between AOM and saline treated rats is seen in Fig. 8(c) and gives an indication of the location of blood supply changes in early stage colon carcinogenesis. Within the range of depths measured by LEBS, an increase in the THb concentration is seen for the AOM-treated rat, a result which is consistent with our previous findings [14,19–22]. The maximum effect occurs at a depth of ~185 μm which corresponds to the base of the colonic crypt. This region is composed of proliferative stems cells which give rise to the epithelial cells lining the crypt and have been implicated as initiators of colon cancer [26,27]. These results therefore suggest that blood supply to the base of the crypt increases in order to satiate the metabolic demands of the proliferating stem cells.
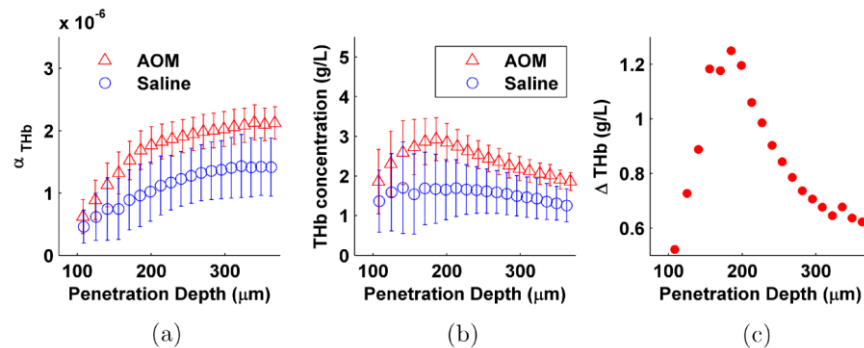


Fig. 8. **[a]** shows the measured total hemoglobin α values for the AOM and saline treated rat specimens across $L_{sc}$. **[b]** shows the measured total hemoglobin concentration as a function of penetration depth. The difference between these two concentration measurements (AOM – Saline) is plotted in **[c]** and indicates the location of the increase in mucosal blood supply.

## 5. Discussion and conclusions

One of the main advantages offered by LEBS for tissue characterization is its ability to selectively interrogate the optical properties at different depths within a layered specimen by changing $L_{sc}$. In this work, we show for the first time that the LEBS peak for a range of different $L_{sc}$ can be reconstructed from the experimental measurement at a single higher $L_{sc}$.

Of particular importance is the ability of the reconstruction method to accurately incorporate the effects of both the scattering and absorption properties in layered media such as biological tissue.

The scattering experiments performed on the spectralon reflectance standard and polystyrene tissue phantom are used to verify the accuracy of the reconstruction method for samples with greatly differing ls*. For the spectralon reflectance standard, the $L_{sc}$ (~153 μm) used for reconstruction is significantly greater than ls* (~20 μm). In this regime, the relative difference between $L_{sc}$ and ls* is large enough that the LEBS readings are virtually insensitive to the sharp changes in $p(r)$ at small length scales due to the phase function. In this case, $p(r)$ is a smoothly changing function with essentially the same shape as would be calculated using the diffusion approximation. For the polystyrene tissue phantom $L_{sc}$ is significantly smaller than ls* (804 μm). In this regime, $p(r)$ has much sharper features at small length scales which are sensitive to the shape of the phase function. In addition, since ls* is so long, the LEBS peak is much shorter and more difficult to distinguish from the noise and CCD artifacts [2]. The accuracy of the reconstructed values for both of these samples indicates that regardless of which regime LEBS measurements are taken from, the reconstruction technique is still valid for a large range of $L_{sc}$.

The validity of the reconstruction method for media containing absorption was verified with liquid Intralipid-hemoglobin phantoms. Using spectral LEBS measurements we accurately reconstructed the shape of the absorption spectrum for a wide range of $L_{sc}$ in both homogenous and two-layered samples. Although the reconstructions at the different $L_{sc}$ represents the information from photons with greatly differing photon path lengths we demonstrate that within the expected physiological range of mucosal hemoglobin concentrations we are able to recover the actual concentration within 5% for all reconstructed $L_{sc}$. This is an important result since it validates the use of a Beer-Lambert law method for quantifying muscosal hemoglobin concentration using LEBS. Applying the reconstruction method towards measurements of colonic tissue from the 10 week AOM-treated rat model of colon carcinogenesis we report an increase in blood supply at a depth corresponding to the base of the colonic crypt. These results are consistent with our previous findings [14,19–22].

It is important to note that the reconstruction method is valid for both homogeneous and layered media, which we demonstrate using a two-layered phantom. Any medium, whether it is homogeneous or layered will have a single $p(r)$ which describes the reflectance profile of scattered light. There are well-established methods for modeling $p(r)$ in multi-layered media using Monte Carlo simulations [28]. For a layered medium, the superficial layers will manifest themselves as alterations in $p(r)$ at small radial separations while the deeper layers will alter $p(r)$ at larger radial separations. Thus, $p(r)$ contains information about the optical properties and depth of each layer within a layered medium. With our reconstruction method, the first step is to measure $p(r)$ for radial separations up to $L_{sc}$. Once we have this measurement of $p(r)$ we are able to accurately reconstruct the LEBS spectrum that would be experimentally measured at a particular $L_{sc}$ as demonstrated in Fig. 7(b). This signal corresponds to the ensemble average of all layers which are sampled by a particular $L_{sc}$.

As discussed above, the LEBS reconstruction method relies on acquiring an accurate representation of $p(r)$ from the experimental LEBS peak. One factor which limits our accuracy in measuring $p(r)$ is the limited angular extent over which we can collect the LEBS peak due to the choice of CCD chip size and focusing lens. Due to the Fourier transform relationship between LEBS and $p(r)$, the limited LEBS angular range corresponds to a loss of resolution in $p(r)$ as well as an inaccuracy at small radial distances. The loss of resolution can be counteracted by zero padding the LEBS peak before recovering $p(r)$. However, since information about the LEBS peak at large angles is not being collected with our current experimental setup, we lose the contribution of these points to the recovered $p(r)$ which translates to a loss of accuracy at length scales smaller than ~50 microns. As such, the reconstruction technique is not valid for very small values of $L_{sc}$ since the resulting peak will

be dominated by the inaccuracies at small radial distances. The obvious conclusion is then to use a CCD chip size and focusing lens which can collect the LEBS peak at large angles. However, this is not always experimentally feasible due to noise considerations. When the LEBS signal is sufficiently above the white noise level produced by the CCD, the angular extent of the peak is limited by the choice of CCD chip size and focusing lens. However, if a large amount of noise is present, the periphery of the peak can fall below the noise floor. In this case, noise becomes the limiting factor for the extent of angular collection and thus can reduce the accuracy of the reconstruction for larger $L_{sc}$. Considering this fact, low-noise LEBS image acquisition is necessary to be able to accurately reconstruct the LEBS peak at small $L_{sc}$.

When using the reconstruction technique for multi-layered media such as biological tissue it is advantageous to take measurements with the longest $L_{sc}$ possible in order to get the most depth information. However, it is still important to consider the tradeoff between acquiring longer $L_{sc}$ measurements and increased acquisition time. While the $L_{sc}$ can be increased by using a smaller secondary source aperture according to $1/a$, the acquisition time (which is inversely proportional to aperture area) increases according to $a^2$. The benefit of this additional acquisition time is that we can readily obtain information from a continuous distribution of smaller $L_{sc}$ and are not just gaining a single point at a longer $L_{sc}$. However, the allowable collection $L_{sc}$ may be limited by the length of time over which measurements can be taken without tissue degradation or due to other practical considerations.

## Acknowledgments